Chemistry
A European
Journal

Chemistry Europe
European Chemical Societies Publishing

Accepted Article

Title: Enhanced performance of CsPbIBr2 perovskite solar cell by modified zinc oxide nanorods array with [6,6]-Phenyl C61 butyric acid

Authors: Jien Yang, Meng Zhang, Qiong Zhang, Chaochao Qin, Ruiping Qin, Sagar M. Jain, and Hairui Liu

To be cited as: *Chem. Eur. J.* **2023**, e202300566

Link to VoR: https://doi.org/10.1002/chem.202300566

WILEY VCH

Chemistry - A European Journal
Volume 29, Issue 40 July 2023, Article number e202300566
DOI:10.1002/chem.202300566

WILEY-VCH

RESEARCH ARTICLE

Enhanced performance of $CsPbIBr_2$ perovskite solar cell by modified zinc oxide nanorods array with [6,6]-Phenyl C_{61} butyric acid

Jien Yang,[a] Meng Zhang,[a] Qiong Zhang,[b] Chaochao Qin,*[b] Ruiping Qin,[a] Sagar M. Jain,*[c] and Hairui Liu*[a]

[a] Dr. J. Yang, M. Zhang, Q. Zhang, Prof. R. Qin, Prof. H. Liu.
College of Material Science and Engineering
Henan Normal University
Xinxiang 453007, China
[b] Dr. C. Qin.
School of Physics
Henan Normal University
Xinxiang 453007, China
[c] Dr. S. Jain.
Concentrated Solar Power Centre for Renewable Energy Systems, School of Water Energy and Environment
Cranfield University
Cranfield MK43 0AL, UK

*The corresponding authors: liuhairui@htu.edu.cn, qinch@hotmail.com, Sagar.M.Jain@cranfield.ac.uk.

Abstract: Although Metal oxide ZnO is widely used as electron transport layers in all-inorganic PSCs due to high electron mobility, high transmittance, and simple preparation processing, the surface defects of ZnO suppress the quality of perovskite film and inhibit the solar cells' performance. In this work, [6,6]-Phenyl C_{61} butyric acid (PCBA) modified zinc oxide nanorods (ZnO NRs) is employed as electron transport layer in perovskite solar cells. The resulting perovskite film coated on the zinc oxide nanorods has better crystallinity and uniformity, facilitating charge carrier transportation, reducing recombination losses, and ultimately improving the cells' performance. The perovskite solar cell with the device configuration of ITO/ZnO nanorods/PCBA/$CsPbIBr_2$/Spiro-OMeTAD/Au delivers a high short circuit current density of 11.83 mA cm^{-2} and power conversion efficiency of 12.05 %.

Introduction

Organic-inorganic perovskite solar cells have experienced prosperous development and achieved a certified power conversion efficiency of more than 25%.[1] Although a high PCE has been achieved, cell stability remains an issue for organic-inorganic hybrid perovskite solar cells, which will limit their use.[2] Replacing the organic cations with suitable inorganic ones would be a feasible solution to this question.[3] Therefore, all-inorganic perovskite solar cells (I-PSCs) have gained popularity and developed rapidly in recent years due to their similar optoelectronic properties and promising stability.[4] In 2012, $CsSnI_3$ was first employed in I-PSCs through a Schottky junction structure.[5] The I-PSC with the conventional device structure was initially reported by Kumar, who utilized $CsSnI_3$ to fabricate the perovskite layer and delivered a PCE of 2.02%.[6] After this, more stable $CsPbX_3$ (X=Cl, Br, I) based PSCs were reported.[7] Cubic phase α-$CsPbI_3$ (black phase) has the narrowest bandgap of 1.73 eV. Unfortunately, it is unsuitable for photovoltaic applications since the black phase of $CsPbI_3$ was probably transformed to yellow phase δ-$CsPbI_3$ at room temperature.[4b] $CsPbI_2Br$ has an appropriate bandgap of ~1.90 eV and achieved a record PCE of 17.8% applied in PSCs recently.[8] Furthermore, $CsPbIBr_2$ has a melting point of around 460 °C and a bandgap of about 2.05eV,[7c] making it suitable for preparing high voltage PSCs, and achieved a PCE of 12% by Liu et al. using a dye molecule VG1-C8 to modify the perovskite film.[9]

In particular, the PSCs usually possess the device structure of perovskite film sandwiched between the electron transport layer (ETL) and hole transport layer (HTL). In I-PSCs, the ETL mainly centers on metal oxides like TiO_2. TiO_2 is the most widely employed ETL in PSCs. However, the high-temperature sintering process required to produce high-quality film hinders the application of TiO_2 on ITO and flexible plastic substrates.[10] Several surface and bulk defects on the surfaces of TiO_2 could affect the performance of PSCs.[11]

ZnO is another candidate for ETL, which has attracted much attention in PSCs as an alternative to the traditional TiO_2. Compared to TiO_2, ZnO has a similar conduction band energy level and possesses higher electronic mobility with excellent transmittance in the visible spectral region, which could facilitate electronic transport, improve the short-circuit current, and reduce recombination loss.[12] Furthermore, previous studies have shown that nano-structured ETLs could improve the performance of PSCs compared to planar structures.[13] ZnO nanorods (ZnO NRs) could be more suitable to use as ETL in perovskite solar cells.[14] Compared with TiO_2, the ZnO NRs as ETL can have a better light harvesting efficiency because NRs can work as

10.1002/chem.202300566

scattering centers; the sunlight reflected by the ZnO NRs results in enhanced absorption of the surrounding perovskite.[15] Law et al. discovered ZnO nanoarrays have hundreds of times higher electron mobility than ZnO nanofilms in DSSC.[16] ZnO nanorods as the electron layer can increase the thickness of the light absorbing layer, enhance light absorption, and thus improve cell performance.[17] However, the perovskite film grown on ZnO would decompose due to the existence of hydroxyl groups or acetate ligands on the metal oxide surface and the proton transfer reactions at the perovskite/ZnO interface.[18] In this case, doping and surface modification are two strategies to ameliorate ZnO. Wang et al. adopted EDTA to chelate with the organic ligands of ZnO, obtained a PCE of 20.38%, and exhibited excellent stability after storage for a period.[19] [6,6]-phenyl C_{61} butyric acid (PCBA), a fullerene derivative, is an excellent electron acceptor. Q. An et al. adopted PCBA as an interfacial modification layer on the surfaces of ZnO nanoparticles to promote perovskite film deposition and improve the devices' PCE.[20] Herein, we demonstrated that the performance of PSC is significantly improved by employing PCBA-modified ZnO NRs as ETL to fabricate PSCs with a novel conventional architecture (ITO/ZnO NRs/PCBA/$CsPbIBr_2$/Spiro-OMeTAD/Au). The approach could obtain a dense perovskite film with big crystal grains and a fully covered ZnO NRs/PCBA interface. Moreover, the modification of ZnO NRs with PCBA could also make the ETL has a better electron extraction capability than other ETLs with a lower carrier recombination rate and finally improve the photovoltaic performance of cells.

Results and Discussion

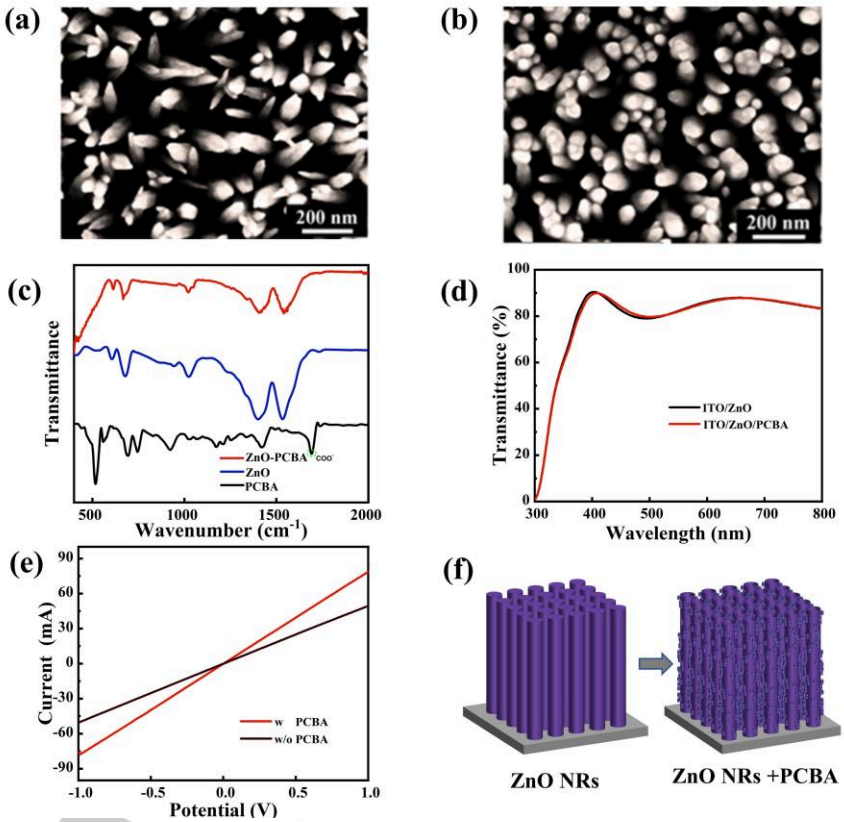

Figure. 1. (a) The top view SEM images of the ZnO NRs without modification of PCBA and (b) modified with PCBA. (c) FTIR spectrums of ZnO, PCBA, and ZnO-PCBA mixed powder. (d) Transmittance spectrums of ITO/ZnO NRs and ITO/ZnO NRs/PCBA. (e) I-V characteristics of ITO/ETL/Ag (f) Schematic diagram of PCBA deposited on ZnO NRs surfaces.

The SEM images of ZnO NRs and ZnO NRs/PCBA are displayed in **Figure. 1a**, **b**. By forming chemical bonds between the carboxyl group and ZnO, the PCBA could anchor on the ZnO NRs' surface.[21] Then, the ZnO NRs are well wrapped up with PCBA, and the cross-section of NRs becomes cylindrical instead of the original conical shape.[14] This configuration is advantageous for charge transport because the NRs could provide a direct pathway for electron transportation. Moreover, the transmission distance is shorter than that of a planar heterojunction.[22] The enhanced charge transport properties could improve the device's photovoltaic performance.[23]

FTIR spectroscopy was selected to study the chemical interaction between PCBA and ZnO. (**Figure. 1c**) PCBA has a characteristic carboxylic acid signal peak of –O–C=O at 1691 cm^{-1}, while when it is mixed with ZnO, the signal is converted to the stretching vibration of carboxylate signals of O-C-O at 1526 cm^{-1} and 1393 cm^{-1}. This result indicates that the hydroxyl or organic ligands of ZnO surface can chelate with PCBA through carboxyl groups, thus optimizing the ZnO surface and then promoting perovskite formation.[24] **Figure. 1d** shows the transmittance spectrums of ZnO NRs with and without PCBA modified. Both samples exhibit high transmission in the visible region, meaning the perovskite

layer can absorb sufficient photons. I-V tests based on the device structures of ITO/ZnO NRs/Ag and ITO/ZnO NRs/PCBA/Ag were performed to compare the conductive properties of ZnO after PCBA modification (**Figure. 1e**). The equation: $\sigma = IL/VA$ can be used to figure up the conductivity (σ) of the device.[25] The value of A is a constant, but L and I/V are different for the two structures. The PCBA-modified device shows a higher L and slope of profile, which indicates a higher conductivity than that of the control. The schematic diagram of depositing PCBA on ZnO NRs surfaces is presented in **Figure. 1f.**

Under the premise of the conventional device structure of ITO/ETL/$CsPbIBr_2$/Spiro-OMeTAD/Au (**Figure. S2a**), the effects of using ZnO NRs and ZnO NRs/PCBA as ETLs on cell performance were investigated. Layered structure with sharp interfaces is noted in the cross-section SEM result of PSCs (**Figure. S2b**). It is shown that the thickness of perovskite is 380 nm, including the infiltration portion in ZnO NRs, and the length of ZnO NRs is about 300 nm. This nanostructure would make the perovskite layer thicker than other planar structures in previous reports.[26]

Unfortunately, the bare ZnO NRs may have some defects, making the perovskite film exist some pinholes or other questions. From the **Figure. 2a**, it is obvious that a few pinholes are scattered on perovskite film deposited on bare ZnO NRs, which can attribute to the presence of hydroxyl groups or acetate ligands on the surfaces of ZnO NRs. Interestingly, a meliorated perovskite film surface morphology without any pinholes is obtained by incorporating PCBA monolayer on the ZnO NRs (**Figure. 2b**). This indicates that modified ZnO NRs with PCBA can improve the penetration of $CsPbIBr_2$. Finally, a dense and no pinholes perovskite film can be obtained, which might improve charge transport properties. The effect of the introduction of PCBA on the crystallization of $CsPbIBr_2$ film can be studied using XRD patterns, and the results are displayed in **Figure. 2c**. The XRD patterns display a series of diffraction peaks at 15.30°, 21.54°, and 30.57°, which index to (110), (112), and (220) planes of an orthorhombic phase of the perovskite, respectively. Furthermore, the result of the pristine film has a (004) diffraction peak at 30.11°, corresponding to the splitting peak of the (220) reflection.[27] In contrast, with the introduction of PCBA, this peak disappears, indicating the excellent crystallinity of perovskite film. All XRD peaks are intensified in the ZnO NRs/PCBA sample, indicating PCBA can promote the crystallinity of perovskite film deposited on ZnO NRs. The self-assembled monolayer of PCBA on ZnO NRs will improve the affinity of the surface to the solvent of DMSO, which can increase the grain size. This result shows agreement with the SEM results (**Figure. 2b**). The full width at half-maximum (FWHM) of XRD peak decreases from 0.149º (w/o PCBA) to 0.119º (w/PCBA) and 0.204º (w/o PCBA) to 0.182º (w/PCBA) at the two primary crystallographic planes (110) and (220), respectively. These changes indicate the presence of PCBA could improve the crystallinity of perovskite film.

The UV-Visible absorption results of $CsPbIBr_2$ films grown on different substrates are displayed in **Figure. 2d**. Compared to bare ZnO NRs, the modified ZnO NRs can load more perovskite materials than that based on the bare ZnO NRs, which can enhance the adsorption in the visible range. The bandgaps of the two samples are obtained by Tauc fitting, and the bandgap decreases from 2.098 eV to 2.094 eV after PCBA modification, which may be favorable for the top junction of the tandem cells. (**Figure. S3**).[28]

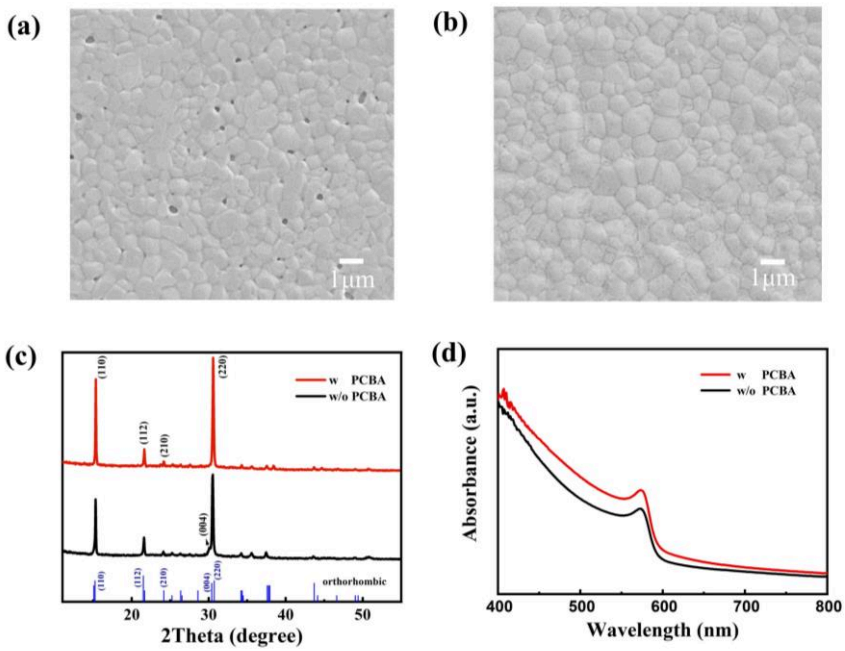

Figure. 2. (a) The top view SEM images of the $CsPbIBr_2$ films on ZnO NRs ETL and (b) ZnO NRs/PCBA ETL. (c) XRD patterns of all-inorganic $CsPbIBr_2$ films on ETL with and without modification with PCBA. (d) The absorption spectra of all-inorganic $CsPbIBr_2$ films on ZnO NRs ETL and ZnO NRs/PCBA ETL.

The steady-state photoluminescence (PL) spectra were measured to investigate the influence of PCBA-modified ZnO NRs on charge carriers in perovskite films. It shows that the perovskite film based on ZnO NRs/PCBA/Glass displays more

efficient PL than based on ZnO NRs/Glass, and the enhanced PL indicates a reduction of nonradiative recombination on modified ZnO NRs, which may be due to the improvement at the interface (**Figure. 3a**),[29] consistent with the results of SEM and XRD **(Figure. 2b, 2c)**. The time-resolved PL spectra of the $CsPbIBr_2$ films deposited on different ETLs are shown in **Figure. 3b**, each result is fitted through a bi-exponential decay function. The slow decay corresponds to the radiative recombination of free carriers, while the fast one relates to defect capturing.[30] Their average value is carrier lifetime (τ_{ave}),[31] and the τ_{ave} of 2.9 ns is obtained for the pristine $CsPbIBr_2$ film. In comparison, it increases to 3.8 ns when the ZnO NRs ETL is employed, and it further increases to 7.8 ns after being modified with PCBA. This result is consistent with the steady-state PL, providing that the ETL modified with PCBA can reduce nonradiative recombination. To learn more about the charge transfer kinetics of perovskite and electron transport layer, we performed the Femtosecond transient absorption (fs-TA) test. The samples were excited by a pump wavelength of 400 nm and a continuous white light of 450~770nm as the probe light. According to **Figure. 3c, 3d,** which represent the pseudo-color TA spectra of perovskite films fabricated on various ETLs, both samples show a negative signal of ground state bleaching (GSB) at 550~570 nm and a positive signal at 570~590 nm of excited state absorption (ESA).[32] When a certain amount of ground-state electrons are excited to the excited state by the pump pulse, the ground state absorption of the probe light will be less than that of the non-excited sample, which will produce a negative signal. **Figure. 3e, 3f** display the spectrums without and with the modification of PCBA under various delay times.[33] At the same delay time, the sample with PCBA modified shows a stronger ground state bleaching peak than the control. Furthermore, with the increasing delay time, the attenuation of the bleach peak of perovskite film with PCBA is faster, which indicates a more efficient carrier transport ability.[34] To describe the decay of perovskite film, we fitted the evolution of the signal at 563 nm as a function of delay time. From the normalized decay kinetic curves in **Figure. S4**, it can be seen that the perovskite film based on ZnO NRs/PCBA shows a faster decay than the control. This result is consistent with the fitted dynamical parameters. The fitted t_2 of ZnO NRs used for ETL is 976.1ps, while with the modification of PCBA, it decreases to 269.4ps (**Table 1**). This result demonstrates that the deposition of PCBA improves the extraction of electrons and consequently promotes cell performance.

Table 1. Fitted dynamical parameters of perovskite films deposited on different ETLs at 563nm.

Sample	t_1	t_2
ZnO NRs/Perovskite	3.518 ns	976.1 ps
ZnO NRs/PCBA/Perovskite	1.651 ns	269.4 ps

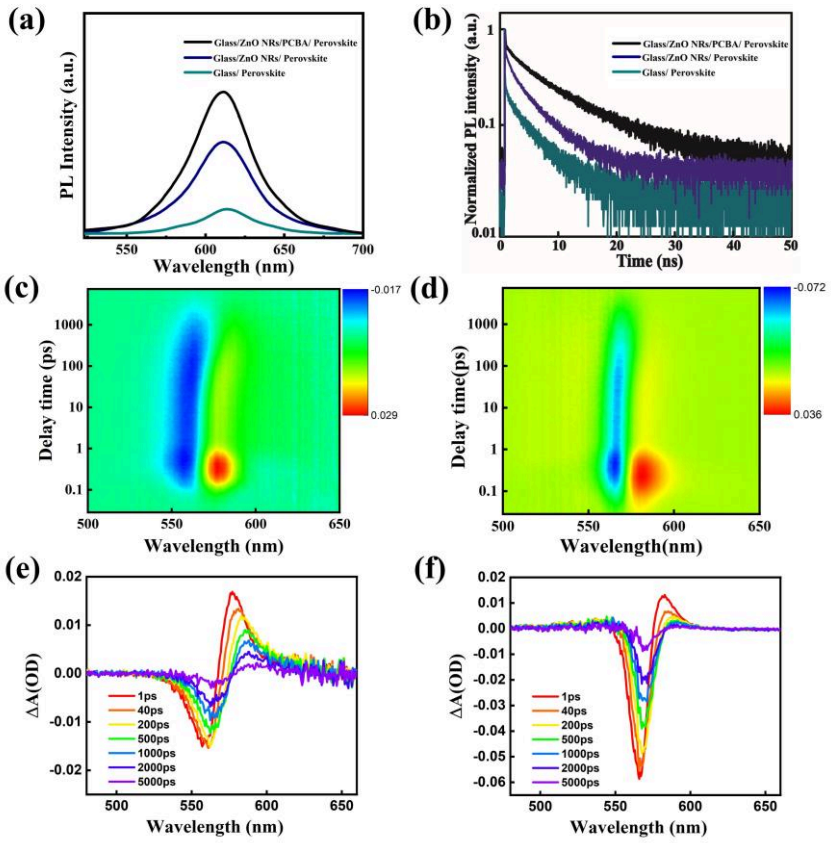

Figure. 3. (a) Steady-state PL spectrums and (b) normalized transient PL decay profiles of perovskite films deposited on glass, glass/ZnO NRs, glass/ZnO NRs/PCBA. The pseudo-color TA spectra of perovskite films grown on (c) ZnO NRs and (d) ZnO NRs/PCBA. TA plots at different delay times for $CsPbIBr_2$ on (e) ZnO NRs and (f) PCBA-modified ZnO NRs.

In addition, we also assessed the defect density and charge transport of these I-PSCs and adopted space-charge-limited current (SCLC) tests. The electron-only devices with the structure of ITO/ZnO NRs/Perovskite/PCBM/Au and ITO/ZnO NRs/PCBA/Perovskite/PCBM/Au were prepared, and the results are shown in **Figure. 4a.** The *J-V* curves divide into three sections: the first named ohmic regime, the second named trap-filling regime, and the third named trap-free SCLC regime.[35] The V_{TFL} of ZnO NRs-based device is 1.694 V, and the value decreases to 1.105 V when PCBA-modified ZnO NRs is employed as ETL. The trap state densities of the devices are calculated to be 1.57×10^{16} cm^{-3} and 2.56×10^{16} cm^{-3} for the perovskite deposited on ZnO NRs/PCBA and ZnO NRs (details are available in supporting information). It can be seen from the result that the deposition of PCBA can reduce trap density and enhance film quality. We also calculate the electron mobility using the equation $J = 9\varepsilon_0\varepsilon_r\mu V^2/8L^3$.[36] The mobility values of the device with ZnO NRs and ZnO NRs/PCBA are estimated to be 9.84 cm^2 V^{-1} S^{-1} and 19.85 cm^2 V^{-1} S^{-1}, respectively. The increased mobility is mainly due to the effective charge transport between ZnO NRs/PCBA ETL and the perovskite layer in I-PSC.

The thermal admittance spectrum tests were carried out, effectively describing the trap density of states (t-DOS) of PSCs. The device structures of ITO/ZnO NRs/$CsPbIBr_2$/Spiro-OMeTAD/Au and ITO/ZnO NRs/PCBA/$CsPbIBr_2$/Spiro-OMeTAD/Au were prepared for the t-DOS test (**Figure. S5.**). The region of 0.3-0.4 eV is the shadow-trap state, corresponding to defects on the surface of perovskite film, and the region of 0.4-0.5 eV is the deep-trap state, corresponding to the defects in the grain boundary. [37] From the result, we can conclude that the device with modified ZnO NRs shows a lower trap state density than the control device throughout the region. The reduction of defect states indicates that the perovskite deposited on the PCBA-modified ZnO NRs has good crystallization and reduced grain boundary defects, consistent with the SCLC result.

The dark *J–V* curves can further confirm the differences in the photovoltaic properties of these devices. Compared with ZnO NRs ETL-based devices, the device based on ZnO NRs/PCBA ETL has a smaller dark current at high bias voltages and smaller leakage current at low bias voltages (**Figure. 4b**). This indicates that the perovskite film based on ZnO NRs/PCBA can improve the current injection, while at the same time preventing leakage current under extremely low voltages.[38]

To investigate the carrier transport properties in PSCs, transient photovoltage (TPV) tests were adopted (**Figure. 4c**). The device with ZnO NRs/PCBA exhibits a slower photovoltage decay than with ZnO NRs, indicating an efficiently suppressed recombination of carriers after PCBA modified. Meanwhile, the transient photocurrent (TPC) measurements were performed, as shown in **Figure. 4d**, compares to the control device, the photocurrent attenuation is significantly faster, conveying a more efficient carrier extraction and transport.[39] These results indicate that the modified ETL will make cells have better carrier dynamic properties, which explains the higher performance of PSCs

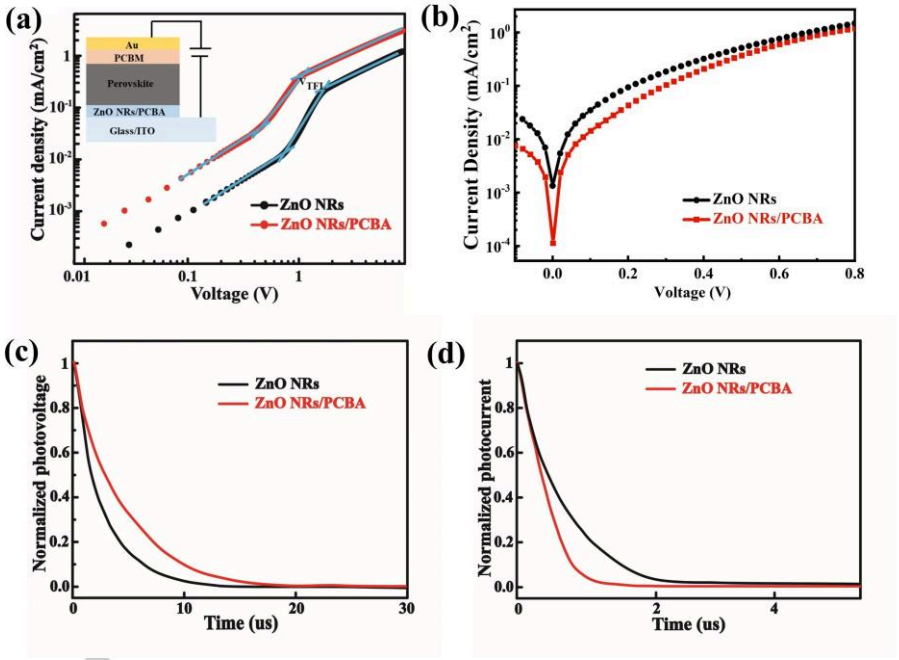

Figure. 4. (a) The SCLC plots of Au/PCBM/perovskite/ETL/ITO devices. (b) Dark *J–V* curves of devices based on different ETLs plotted on a semilog scale. (c) TPV decay curves, (d) TPC decay curves for ZnO NRs- and ZnO NRs/PCBA-based $CsPbIBr_2$ PSCs.

The *J-V* curves of the devices measured after optimization are shown in **Figure. 5a**. **Table 2** provides the detailed performance parameters of devices with different ETLs. It is clear from the table that the modified device shows higher performance parameters than using ZnO NRs as ETL, and the champion device achieves a V_{oc} of 1.30 V, a J_{sc} of 11.83 mA cm^{-2}, a FF of 78.41%, and a PCE of 12.05%. The performance parameter statistics of 18 devices based on different ETLs are shown in **Figure. S6**. The significant PCE increase mainly depends on the improvement in J_{sc} and V_{oc}, which may result from the enhanced light absorption capacity and faster charge transport process caused by PCBA-modified ZnO NRs as ETL. **Figure. 5b** displays the EQE spectra of the champion device based on different fabrications. This spectrum shows that the device modified with PCBA exhibits a

higher EQE among the wavelength of 300~600nm, demonstrating a more efficient light absorption in the visible range. The EQE intensity of the PSCs with ZnO NRs/PCBA is used to calculate the integrated J_{sc}, and the result of the champion device is 11.08 mA cm^{-2}, which agrees well with the J-V curve. The integrated J_{sc} values obtained from EQE curves are approximations of *J–V* curves, indicating a valid measurement of the latter, which delivers a well photoelectric conversion performance.

For PSCs, it is a crucial feature that converts solar energy into electricity to a great extent. For this purpose, the power output of the champion devices is evaluated under maximum power-point conditions.[40] Optimizing the device made the PCE output stable at 11.57% of the PCBA-modified device and 9.05% of the control device (**Figure. 5c.**). The stabilized efficiency obtained for the I-PSCs can be attributed to the inhibition of ion motion or surface charge trapping by PCBA.

Finally, the PSCs′ long-term stability was further investigated. The effect of the addition of PCBA on the device′s stability is evaluated, and the results are displayed in **Figure. 5d.** Unencapsulated cells were stored under identical conditions (30 ºC, relative humidity around 40-45%) and tested every 50 hours. From the schematic diagrams, we can obtain that after 300 hours of storage, the device based on modified ZnO NRs might maintain 85% of the original efficiency. In contrast, the control device's efficiency gradually decreases and shows about 63% degradation. This result coincides with the photographs of perovskite films on different ETLs at different times. After storing for 300h, the PCBA-modified perovskite film shows slower degradation than the control. Perovskite is very sensitive to oxygen and water and susceptible to degradation. The existence of pinholes in the film will provide moisture or oxygen with more sites to contact perovskite, which can accelerate the decomposition of perovskite devices.[41] Therefore, the modified perovskite forms a continuous structure without pinholes, thus improving the stability of the device under environmental conditions.

Table 2. Device photovoltaic performance of perovskite films based on ZnO NRs ETL, and ZnO NRs/PCBA ETL.

ETL	V_{oc} (V)	J_{sc} (mA cm^{-2})	FF (%)	PCE (%)
ZnO NRs	1.21	11.23	71.73	9.74
ZnO NRs/PCBA	1.30	11.83	78.41	12.05

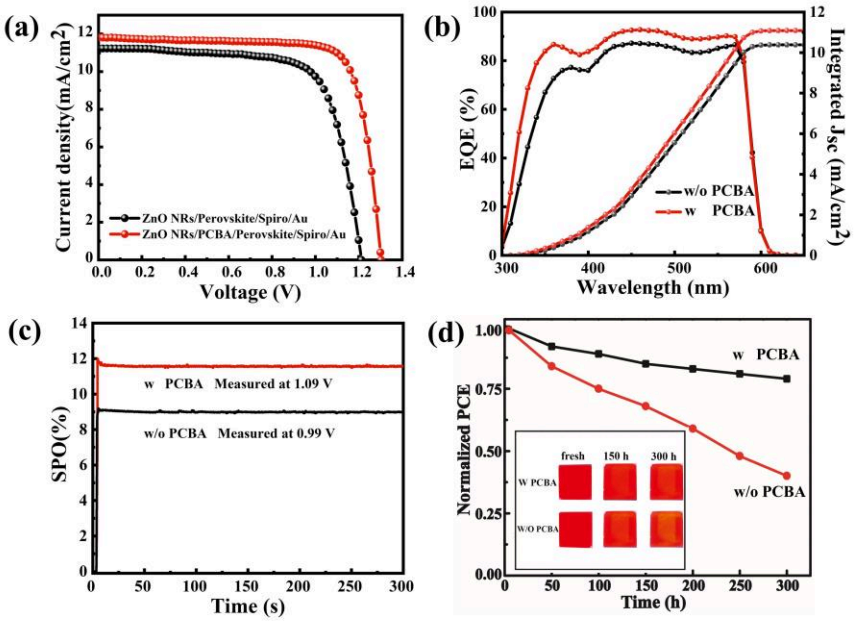

Figure. 5. (a) The *J–V* curves of all-inorganic $CsPbIBr_2$ PSCs on different ETLs. (b) The EQE spectrums and integrated J_{sc} of the champion device. (c) The time-dependent stabilized power output of the champion devices grown on ZnO NRs and ZnO NRs/PCBA. (d) Stability tests in ambient conditions. The inset shows the photographs of perovskite films on different ETLs at different times.

Conclusion

In summary, our work introduces PBCA to modify ZnO NRs, reduce surface defects, optimize perovskite film morphology, and enhance charge extraction properties. After modification of PCBA, performing a full coverage $CsPbIBr_2$ perovskite film on the ZnO NRs substrate is simple. The optimized structure could improve optical absorption and enhance the capability of electron extraction, which could positively affect the extraction of photogenerated carriers in PSC, thereby promoting the photovoltaic performance of the device. Generally, the V_{oc} of the optimized device increases to 1.30 V, and the champion PCE is 12.05%. This study provides an interfacial modified method that would further improve the efficiency of the PSCs in the future.

Experimental Section

Materials: Experimental materials include ITO, ethylene glycol monomethyl ether, ethanol amine, NaOH, $Zn(NO_3)_2{\cdot}6H_2O$, $Zn(CH_3COO)_2{\cdot}2H_2O$, CsI, Dimethyl sulfoxide, chlorobenzene, acetonitrile, $PbBr_2$, Spiro-OMeTAD, LiTFSI, TBP, PCBA. Detailed specifications and sources can be found in the supporting information.

Fabrication of Perovskite Solar Cells: The conventional device structures of ITO/ETL/Perovskite/Spiro-OMeTAD/Au were prepared, and a PCBA interface layer was added to modify ZnO NRs electron transport layer. Details of the preparation process are in the supporting information.

Characterizations: The detailed characterization description can be seen in supporting information.

Acknowledgments

This work was supported by the Henan Province college youth backbone teacher project (No: 2020GGJS062), the Basic Research Project of Key Scientific Research Project of Henan Province (21A430023) and the Youth Science Foundation of Henan Province (202300410239).

Keywords: Zinc oxide nanorods • inorganic $CsPbIBr_2$ perovskite solar cell • interface modification • [6,6]-Phenyl C_{61} butyric acid

References

[1] a) L. Ji, S. Sun, Y. Qin, K. Li, W. Li, *Coord. Chem. Rev.* **2019**, *391*, 15-29; b) C. Mai, Q. Xiong, X. Li, J. Chen, J. Chen, C. Chen, J. Xu, C. Liu, C. Y. Yeh, P. Gao, *Angew. Chem. Int. Ed.* **2022**, e202209365; c) A. Wang, C. Zuo, X. Niu, L. Ding, J. Ding, F. Hao, *Chem. Eng. J.* **2022**, *451*, 138926.

[2] a) F. Wei, R. Antonio Gaetano, A. A. Quinten, J. Rohit Abraham, T. Mohammad Mahdi, E. Stephanie, V. K. Maksym, S. Michael, *Mater. Today* **2022**; b) J. Y. L. Vincent, M. U. Aleksander, K. Christina, T. K. Matthew, P. Laura Miranda, B. J. Michael, M. H. Laura, *Adv. Energy Mater.* **2022**, 2200847.

[3] S. Zhou, R. Tang, L. Yin, *Adv. Mater.* **2017**, *29*, 1703682.

[4] a) J. Tian, Q. Xue, Q. Yao, N. Li, C. J. Brabec, H. L. Yip, *Adv. Energy Mater.* **2020**, *10*, 2000183; b) S. Kajal, G.-H. Kim, C. W. Myung, Y. S. Shin, J. Kim, J. Jeong, A. Jana, J. Y. Kim, K. S. Kim, *J. Mater. Chem. A* **2019**, *7*, 21740-21746; c) J. Duan, H. Xu, W. E. I. Sha, Y. Zhao, Y. Wang, X. Yang, Q. Tang, *J. Mater. Chem. A* **2019**, *7*, 21036-21068.

[5] Z. Chen, J. Wang, Y. Ren, C. Yu, K. Shum, *Appl. Phys. Lett.* **2012**, *101*, 093901.

[6] M. H. Kumar, S. Dharani, W. L. Leong, P. P. Boix, R. R. Prabhakar, T. Baikie, C. Shi, H. Ding, R. Ramesh, M. Asta, M. Graetzel, S. G. Mhaisalkar, N. Mathews, *Adv. Mater.* **2014**, *26*, 7122-7127.

[7] a) J. Zhang, G. Hodes, Z. Jin, S. F. Liu, *Angew. Chem. Int. Ed.* **2019**, *58*, 15596-15618; b) W. Chen, X. Li, Y. Li, Y. Li, *Energy Environ. Sci.* **2020**, *13*, 1971-1996; c) Y. Guo, X. Yin, J. Liu, W. Que, *J. Mater. Chem. A* **2019**, *7*, 19008-19016; d) C. Liu, Y. Yang, O. A. Syzgantseva, Y. Ding, M. A. Syzgantseva, X. Zhang, A. M. Asiri, S. Dai, M. K. Nazeeruddin, *Adv. Mater.* **2020**, *32*, 2002632.

[8] Y. Ding, Q. Guo, Y. Geng, Z. Dai, Z. Wang, Z. Chen, Q. Guo, Z. Zheng, Y. Li, E. Zhou, *Nano Today* **2022**, *46*, 101586.

[9] Q. Liu, J. Qiu, X. Yan, Y. Fei, Y. Qiang, Q. Chang, Y. Wei, X. Zhang, W. Tian, S. Jin, Z. Yu, L. Sun, *J. Energy Chem.* **2022**, *74*, 387-393.

[10] J. Nam, J. H. Kim, C. S. Kim, J. D. Kwon, S. Jo, *ACS Appl. Mater. Interfaces* **2020**, *12*, 12648-12655.

[11] W. Hu, S. Yang, S. Yang, *Trends in Chemistry* **2019**, *2*, 148-162.

[12] L. Lin, T. W. Jones, T. C. J. Yang, N. W. Duffy, J. Li, L. Zhao, B. Chi, X. Wang, G. J. Wilson, *Adv. Funct. Mater.* **2020**, *31*, 2008300.

[13] a) M. Matshidiso, S. M. Bernard, O. O. Richard, E. M. Tshwafo, D. M. Thembinkosi, *Processes* **2022**, *10*, 1803; b) S. Li, P. Zhang, Y. Wang, H. Sarvari, D. Liu, J. Wu, Y. Yang, Z. Wang, Z. Chen, *Nano Res.* **2017**, *10*, 1092-1103.

[14] Y. Xu, Y. Wang, J. Yu, B. Feng, H. Zhou, J. Zhang, J. Duan, X. Fan, P. A. V. Aken, P. D. Lund, *IEEE J. Photovolt.* **2016**, *6*, 1530-1536.

[15] Z. Liu, T. He, H. Wang, S. M. Jain, K. Liu, J. Yang, N. Zhang, H. Liu, M. Yuan, *J. Power Sources* **2018**, *401*, 303-311.

[16] M. Law, L. E. Greene, J. C. Johnson, R. Saykally, P. Yang, *Nat. Mater.* **2005**, *4*, 455-459.

[17] Z. Liang, Q. Zhang, L. Jiang, G. Cao, *Energy Environ. Sci.* **2015**, *8*, 3442-3476.

[18] a) Y. Dkhissi, S. Meyer, D. Chen, H. C. Weerasinghe, L. Spiccia, Y.-B. Cheng, R. A. Caruso, *ChemSusChem* **2016**, *9*, 687-695; b) J. Yang, B. D. Siempelkamp, E. Mosconi, F. De Angelis, T. L. Kelly, *Chem. Mater.* **2015**, *27*, 4229-4236.

[19] Z. Wang, X. Zhu, J. Feng, C. Wang, C. Zhang, X. Ren, S. Priya, S. Liu, D. Yang, *Adv. Sci.* **2021**, *8*, 2002860.

[20] Q. An, P. Fassl, Y. J. Hofstetter, D. Becker-Koch, A. Bausch, P. E. Hopkinson, Y. Vaynzof, *Nano Energy* **2017**, *39*, 400-408.

[21] Y. Dong, W. Li, X. Zhang, Q. Xu, Q. Liu, C. Li, Z. Bo, *Small* **2016**, *12*, 1098-1104.

[22] F. Shahvaranfard, M. Altomare, Y. Hou, S. Hejazi, W. Meng, B. Osuagwu, N. Li, C. J. Brabec, P. Schmuki, *Adv. Funct. Mater.* **2020**, *30*, 1909738.

[23] H. Li, C. Chen, H. Hu, Y. Li, Z. Shen, F. Li, Y. Liu, R. Liu, J. Chen, C. Dong, S. Mabrouk, R. S. Bobba, A. Baniya, M. Wang, Q. Qiao, *InfoMat* **2022**, *4*, e12322.

[24] a) J. Ryczkowski, *Appl. Surf. Sci.* **2005**, *252*, 813-822; b) X. Li, X. Liu, W. Zhang, H. Wang, J. Fang, *Chem. Mater.* **2017**, *29*, 4176-4180; c) Z. Wang, X. Zhu, J. Feng, C. Wang, C. Zhang, X. Ren, S. Priya, S. Liu, D. Yang, *Adv. Sci.* **2021**, *8*, 2002860.

[25] a) J. H. Heo, M. H. Lee, H. J. Han, B. R. Patil, J. S. Yu, S. H. Im, *J. Mater. Chem. A* **2016**, *4*, 1572-1578; b) Y. Huang, S. Li, C. Wu, S. Wang, C. Wang, R. Ma, *New J. Chem.* **2020**, *44*, 8902-8909.

[26] M. Wu, Y. Lin, S. Chen, M. Jao, Y. Chang, K. M. Lee, C. Lai, Y. Chen, W. Su, *Small* **2020**, *16*, 2002201.

[27] M. Rodová, J. Brožek, K. Knížek, K. Nitsch, *J. Therm. Anal. Calorim.* **2003**, *71*, 667-673.

[28] a) S. Tan, B. Yu, Y. Cui, F. Meng, C. Huang, Y. Li, Z. Chen, H. Wu, J. Shi, Y. Luo, D. Li, Q. Meng, *Angew. Chem. Int. Ed.* **2022**, *61*, e202201300; b) M. T. Hörantner, T. Leijtens, M. E. Ziffer, G. E. Eperon, M. G. Christoforo, M. D. McGehee, H. J. Snaith, *ACS Energy Lett.* **2017**, *2*, 2506-2513.

[29] a) T. Kirchartz, J. A. Márquez, M. Stolterfoht, T. Unold, *Adv. Energy Mater.* **2020**, *10*, 1904134; b) W. Zhu, Z. Zhang, D. Chen, W. Chai, D. Chen, J. Zhang, C. Zhang, Y. Hao, *Nanomicro Lett.* **2020**, *12*, 87; c) Q. Zhou, D. He, Q. Zhuang, B. Liu, R. Li, H. Li, Z. Zhang, H. Yang, P. Zhao, Y. He, Z. Zang, J. Chen, *Adv. Funct. Mater.* **2022**, *32*, 2205507.

[30] S. Cacovich, P. Dally, G. Vidon, M. Legrand, S. Gbegnon, J. Rousset, J.-B. Puel, J.-F. Guillemoles, P. Schulz, M. Bouttemy, A. Etcheberry, *ACS Appl. Mater. Interfaces* **2022**, *14*, 34228-34237.

[31] V. Adinolfi, W. Peng, G. Walters, O. M. Bakr, E. H. Sargent, *Adv. Mater.* **2018**, *30*, 1700764.

[32] a) X. Liu, Z. Yu, T. Wang, K. L. Chiu, F. Lin, H. Gong, L. Ding, Y. Cheng, *Adv. Energy Mater.* **2020**, *10*, 2001958; b) K. Pydzińska, J. Karolczak, I. Kosta, R. Tena-Zaera, A. Todinova, J. Idígoras, J. A. Anta, M. Ziółek, *ChemSusChem* **2016**, *9*, 1647-1659; c) J. S. Manser, P. V. Kamat, *Nat. Photonics* **2014**, *8*, 737-743.

[33] C. Wang, Y. Liu, Y. Guo, L. Ma, Y. Liu, C. Zhou, X. Yu, G. Zhao, *Chem. Eng. J.* **2020**, *397*, 125367.

[34] a) X. Zhu, C. F. J. Lau, K. Mo, S. Cheng, Y. Xu, R. Li, C. Wang, Q. Zheng, Y. Liu, T. Wang, Q. Lin, Z. Wang, *Nano Energy* **2022**, *103*, 107849; b) H. Liu, Z. Zhang, Z. Su, W. Zuo, Y. Tang, F. Yang, X. Zhang, C. Qin, J. Yang, Z. Li, M. Li, *Adv. Sci.* **2022**, *9*, 2105739.

[35] a) D. Moia, I. Gelmetti, P. Calado, Y. Hu, X. Li, P. Docampo, J. de Mello, J. Maier, J. Nelson, P. R. F. Barnes, *Phys. Rev. Applied* **2022**, *18*, 044056; b) E. A. Duijnstee, J. M. Ball, V. M. Le Corre, L. J. A. Koster, H. J. Snaith, J. Lim, *ACS Energy Lett.* **2020**, *5*, 376-384. c) V. M. Le Corre, E. A. Duijnstee, O. El Tambouli, J. M. Ball, H. J. Snaith, J. Lim, L. J. A. Koster, *ACS Energy Lett.* **2021**, *6*, 1087-1094.

[36] Q. Zhou, J. Du, J. Duan, Y. Wang, X. Yang, Y. Duan, Q. Tang, *J. Mater. Chem. A* **2020**, *8*, 7784-7791.

[37] a) W. Chen, Y. Zhou, G. Chen, Y. Wu, B. Tu, F. Liu, L. Huang, A. M. C. Ng, A. B. Djurišić, Z. He, *Adv. Energy Mater.* **2019**, *9*, 1803872. b) X. Zheng, B. Chen, J. Dai, Y. Fang, Y. Bai, Y. Lin, H. Wei, X. Zeng, J. Huang, *Nat. Energy* **2017**, *2*, 17102.

[38] A. A. Khan, M. Azam, D. Eric, G. Liang, Z. Yu, *J. Mater. Chem. C* **2020**, *8*, 2880-2887.

[39] J. Jiménez-López, B. M. D. Puscher, D. M. Guldi, E. Palomares, *J. Am. Chem. Soc.* **2019**, *142*, 1236-1246.

[40] S. N. Habisreutinger, N. K. Noel, H. J. Snaith, *ACS Energy Lett.* **2018**, *3*, 2472-2476.

[41] S. Chen, X. Dai, S. Xu, H. Jiao, L. Zhao, J. Huang, *Science* **2021**, *373*, 902-907.

10.1002/chem.202300566

Table of Contents:

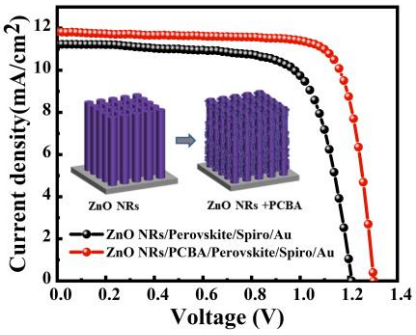

[6,6]-Phenyl C_{61} butyric acid (PBCA) is introduced to modify ZnO nanorods (ZnO NRs) electron transport layer to reduce surface defects, ameliorate the morphology of perovskite film, enhance charge extraction properties, and improve the photovoltaic performance of $CsPbIBr_2$ perovskite solar cells.